ARMY RESEARCH LABORATORY

Evaluating a Multivariate Directional Connectivity Measure for Use in Electroencephalogram (EEG) Network Analysis Using a Conductance-Based Neuron Network Model

by Jean M Vettel and Piotr J Franaszczuk

ARL-TR-7232 **March 2015**

Approved for public release; distribution is unlimited.

NOTICES

Disclaimers

The findings in this report are not to be construed as an official Department of the Army position unless so designated by other authorized documents.

Citation of manufacturer's or trade names does not constitute an official endorsement or approval of the use thereof.

Destroy this report when it is no longer needed. Do not return it to the originator.

Army Research Laboratory
Aberdeen Proving Ground, MD 21005-5425

ARL-TR-7232 **March 2015**

Evaluating a Multivariate Directional Connectivity Measure for Use in Electroencephalogram (EEG) Network Analysis Using a Conductance-Based Neuron Network Model

Jean M Vettel
Human Research and Engineering Directorate, ARL
University of California Santa Barbara

Piotr J Franaszczuk
Human Research and Engineering Directorate, ARL
The Johns Hopkins University

Approved for public release; distribution is unlimited.

REPORT DOCUMENTATION PAGE

Form Approved
OMB No. 0704-0188

Public reporting burden for this collection of information is estimated to average 1 hour per response, including the time for reviewing instructions, searching existing data sources, gathering and maintaining the data needed, and completing and reviewing the collection information. Send comments regarding this burden estimate or any other aspect of this collection of information, including suggestions for reducing the burden, to Department of Defense, Washington Headquarters Services, Directorate for Information Operations and Reports (0704-0188), 1215 Jefferson Davis Highway, Suite 1204, Arlington, VA 22202-4302. Respondents should be aware that notwithstanding any other provision of law, no person shall be subject to any penalty for failing to comply with a collection of information if it does not display a currently valid OMB control number.
PLEASE DO NOT RETURN YOUR FORM TO THE ABOVE ADDRESS.

1. REPORT DATE *(DD-MM-YYYY)*	2. REPORT TYPE	3. DATES COVERED (From - To)
March 2015	Final	January 2011–December 2013

4. TITLE AND SUBTITLE
Evaluating a Multivariate Directional Connectivity Measure for Use in Electroencephalogram (EEG) Network Analysis Using a Conductance-Based Neuron Network Model

5a. CONTRACT NUMBER

5b. GRANT NUMBER

5c. PROGRAM ELEMENT NUMBER

6. AUTHOR(S)
Jean M Vettel and Piotr J Franaszczuk

5d. PROJECT NUMBER

5e. TASK NUMBER

5f. WORK UNIT NUMBER

7. PERFORMING ORGANIZATION NAME(S) AND ADDRESS(ES)
US Army Research Laboratory
ATTN: RDRL-HRS-C
Aberdeen Proving Ground, MD 21005-5425

8. PERFORMING ORGANIZATION REPORT NUMBER
ARL-TR-7232

9. SPONSORING/MONITORING AGENCY NAME(S) AND ADDRESS(ES)

10. SPONSOR/MONITOR'S ACRONYM(S)

11. SPONSOR/MONITOR'S REPORT NUMBER(S)

12. DISTRIBUTION/AVAILABILITY STATEMENT
Approved for public release; distribution is unlimited.

13. SUPPLEMENTARY NOTES

14. ABSTRACT
Neuroscientists have shown increasing interest in understanding brain networks, and directional connectivity measures based on multivariate autoregressive (MVAR) models of signals have been proposed as a method to recover patterns of functional brain connectivity. In the past, the mathematical properties of these measures have been studied by applying them to well-defined linear models or differential equations describing nonlinear oscillations. Our work tests these measures on more realistic electroencephalogram (EEG) signals to evaluate their applicability for experimental use. This report evaluates how well an effective functional connectivity measure, the directed transfer function (DTF), captures the connectivity patterns across 6 simulated 4-node networks. Each node in the network is composed of conductance-based model neurons that have been tuned to oscillate in frequency bands common in experimental EEG studies, alpha and gamma. The resulting time series from each simulation was separately modeled using multivariate autoregressive modeling, and DTF was computed from the model coefficients. Our results demonstrate that this measure can lead to spurious results in both simple feed forward networks and more complex networks with feedback loops and a ring structure; however, we propose 2 guiding principles that can increase the reliability of the results and discuss their applicability and interpretability for future EEG experimental analyses.

15. SUBJECT TERMS
conductance-based neuron models, directed transfer function, DTF, brain networks, connectivity

16. SECURITY CLASSIFICATION OF:			17. LIMITATION OF ABSTRACT	18. NUMBER OF PAGES	19a. NAME OF RESPONSIBLE PERSON
a. REPORT	b. ABSTRACT	c. THIS PAGE			Jean M Vettel
Unclassified	Unclassified	Unclassified	UU	42	19b. TELEPHONE NUMBER (*Include area code*) 410-278-7431

Standard Form 298 (Rev. 8/98)
Prescribed by ANSI Std. Z39.18

Contents

List of Figures

List of Tables

Acknowledgments

The authors would like to acknowledge the contribution by Alexander Urban to this project; he implemented portions of the simulation, analyzed the time series data, created all of the figures, and wrote sections of an earlier version of this manuscript. The authors would also like to acknowledge the helpful feedback and suggested revisions from 4 technical reviewers as well as informal science discussions about this work with colleagues at the Translational Neuroscience Branch at the US Army Research Laboratory. Research was sponsored by the US Army Research Laboratory, and Urban was supported under Cooperative Agreement Number W911NF-12-2-0019.

1. Introduction

Neuroscientists have shown increasing interest in recent years in examining the integrated activity of the brain's circuitry across large-scale networks (Sporns et al. 2004; Friston 2011; Alivisatos et al. 2012). This idea is based on the notion that functional connections are formed through synchronously firing assemblies (populations) of neurons (e.g., Engel et al. 2001; Varela et al. 2001), and experimentalists have identified several frequency bands, such as alpha and gamma, that relate changes in ongoing brain oscillations to behavioral performance (Klimesch et al. 2007; Jensen et al. 2012). These functional connections are dynamically changing, and within short time periods, connections between neural populations can be created, broken, and reestablished with other populations in response to different sensory stimuli and different processing demands (Battaglia et al. 2012; Buschman et al. 2012). Given the importance of these functional networks for communication across brain regions, electroencephalogram (EEG) experiments have increasingly focused on linking variability in functional networks to performance on behavioral tasks (Supp et al. 2005; Philiastides and Sajda 2006; Sun et al. 2009; Sakkalis 2011; Ioannides et al. 2012; Blinowska et al. 2013).

Researchers have attempted to devise different approaches and methods for measuring functional networks accurately in EEG time series that are robust to noise. One class of functional measures known as effective connectivity refers to directed interactions between different brain regions or cell populations, and it is closely related to the concept of generalized synchronization (Schiff et al. 1996; Battaglia et al. 2012). There are a variety of signal analysis measures used for trying to detect effective connections between different neural populations, including Kullback-Leibler Divergence, Transfer Entropy, Partial Directed Coherence, Directed Transfer Function (DTF), and the direct DTF (for review, see Blinowska-Cieślak and Zygierewicz 2012; Seghouane and Amari 2012). In this analysis, we focus on DTF, which is related to the concept of Granger Causality and derived from multivariate autoregressive modeling (MVAR) of the time series. Granger-Geweke causality was originally introduced in economic time series analysis and used to study dependencies in bivariate signals (Granger 1969; Geweke 1982). If incorporating the components of the model of the first signal helps reduce the error of prediction in the second signal, the first signal is said to have caused the second signal. Thus these effective connectivity measures hold promise for capturing the temporal dynamics of functional neural networks (Blinowska et al. 2013).

This study investigates how well DTF, an effective connectivity measure, captures the underlying network connectivity of a simulated, EEG-like signal generated from several thousand nonlinear conductance-based neuron models. We simulate 6 different networks, each with 4 interacting nodes that oscillate within 2 frequency bands of interest in experimental EEG studies, alpha and gamma (Nunez and Srinivasan 2006). Four of the networks are simple

feed-forward networks with one node driving 3 other nodes, and we manipulate whether the driving or receiving nodes oscillate at alpha or gamma frequencies. Two of the networks have a more complex connectivity pattern and include feedback connections and a ring structure.

Our evaluation of these measures differs from the previous studies, which have used multichannel signals generated by MVAR models with defined dependencies in the coefficients (Baccalá and Sameshima 2001) or periodic signals with introduced delays between channels as a means of validating the measures (Blinowska et al. 2013). In other studies, bivariate connectivity measures were validated using neural mass models (David and Friston 2003; Wendling et al. 2009). In the present study, we investigate the multichannel directional connectivity measure related to Granger causality applied to signals generated from 4-node networks. Since the simulated signals are created as a superposition of post-synaptic potentials of conductance-based models of neurons, our model better resembles an experimental EEG signal, which is created by the activity of firing neurons.

From the results, we propose 2 guiding principles for the application of effective connectivity measures to experimental data to minimize spurious connections: computing the measure only when there is overlapping power in the spectrum and applying a conservative statistical threshold. Interpretation of these connectivity results can be further enhanced by incorporating known anatomical constraints.

2. Methods

2.1 Neural Networks Generating EEG-like Signals

The simulated neural signals were generated using a modified version (Suffczynski et al. 2014) of the cortical network model originally developed to study epileptic phenomena (Kudela et al. 1997; Anderson et al. 2012). The modifications included changes to simulate normal cortical activity without inducing seizures. This implementation integrates nonlinear conductance-based neuron model equations using Euler's method with a fixed step size of 0.01 ms.

The model networks we examined all consist of 4 interacting nodes, each node consisting of a 2-layer model of 400 excitatory neurons (pyramidal cells) and 100 inhibitory interneurons. A schematic of the arrangement as well as connectivity between layers is illustrated in Fig. 1. The current balance equation for the excitatory neurons has the form

$$C\frac{dV}{dt} = -I_{syn} - I_{Na} - I_{Ca} - I_K - I_K(Ca) - I_A - I_L. \quad (1)$$

The form of the equations for the inhibitory interneurons is identical to the excitatory neurons except for the deletion of the calcium-dependent potassium current (Suffczynski et al. 2014). The detailed equations and symbols definitions are provided in Appendix A.

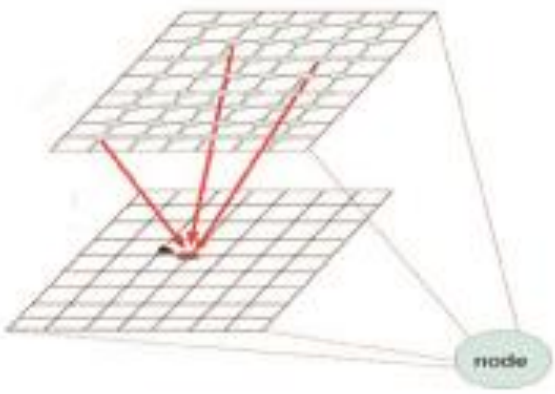

Fig. 1 A simulated node consists of 400 excitatory neurons and 100 inhibitory neurons. Connectivity between and within layers were randomly chosen. Example consists of one neuron in one layer connected to 3 neurons in another layer.

For each node, connections among the 500 neurons were chosen randomly from a uniform distribution that ensures connections between all neurons were equally likely. Each connection was one of 4 possible types: excitatory to excitatory, excitatory to inhibitory, inhibitory to inhibitory, and inhibitory to excitatory. The connection strength and delay between the neurons was also randomly selected from a Gaussian distribution. In addition to these connections within each node, a total of 120 connections were randomly selected between each node pair to create the small networks used in the simulations. The model equations and connectivity parameters are provided in Appendix A.

To generate different frequency oscillations in the simulated networks, we set different levels of stimulation to different nodes. The stimulation to each node was generated by a Poisson process of action potentials to the excitatory cells. By varying the rate parameter λ of the Poisson process, we can shift the frequency of the node's synchronous oscillation. Model parameters were chosen so that their power spectra peaked within 2 experimentally relevant frequency bands (Nunez and Srinivasan 2006): approximately 11 Hz to represent the alpha band and approximately 40 Hz to represent the gamma band.

The resulting oscillatory signal from each node was modeled as an EEG-like signal by summing and low-pass filtering the postsynaptic potentials of all excitatory synapses (Nunez and Srinivasan 2006; Suffczynski et al. 2014). For each node, 5 s of simulated signals are generated from summation of the postsynaptic potentials, and then they are filtered using a low-pass Butterworth filter of order 10 with cut-off at 100 Hz and decimated. The first and last 50 ms are discarded in the filtering process. This procedure resulted in simulated signal with a sampling frequency of 200 Hz. The resulting signal used in the effective connectivity analysis consisted of 980 points. This length of the signal window also fulfills constraints for computing an MVAR model, ensuring that the number of estimated coefficients is less than 1/10th of the total number of points (Blinowska-Cieślak and Zygierewicz 2012).

We used this procedure to generate 6 simulated networks that were either simple feed-forward networks or more complex feedback networks. Each network had 4 nodes. The 4 simple networks have one node projecting to 3 other nodes, and we vary whether the sending or receiving nodes oscillate within alpha or gamma frequency bands. The 2 complex networks have feedback connections and a ring structure among the nodes, and we again vary whether the sending and receiving nodes oscillate at alpha or gamma.

2.2 Effective Connectivity Measure

The time series from 6 simulated EEG-like networks were analyzed separately using an effective connectivity measure, DTF. Related to Granger-Geweke causality (Granger 1969; Geweke 1982), this measure is based on MVAR modeling of time series and have been interpreted as a multivariate extension of the Granger concept (Baccalá and Sameshima 2001; Korzeniewska et al. 2003; Blinowska 2011; Blinowska-Cieślak and Zygierewicz 2012; Haufe et al. 2013). When the time series data are fit to an autoregressive model by minimizing the error terms, the model coefficients provide information about time lag influences between the signals and thus capture the connections producing those signals. We examine how well DTF captures the underlying connectivity among the nodes in our simulated EEG-like networks.

The simulated signals for each network were separately modeled as an MVAR process; that is, we assume that the signals can be described as

$$\vec{x}(n) = \sum_{k=1}^{p} \boldsymbol{A}(k)\, \vec{x}(n-k) + \vec{w}(n). \qquad (2)$$

In this equation, p is the model order and $w(n)$ is interpreted as a white noise process or the error in the prediction. We solve for the matrix model coefficients $\boldsymbol{A}(k)$ by noting that $x(n-k)$ is uncorrelated to $w(n)$. This allows us to write the equations as a block-Toeplitz matrix problem, which can be solved by the Levinson-Wiggins-Robinson (LWR) algorithm. More details on this derivation or the LWR algorithm can be found in Golub and Loan (2012).

Connectivity is then calculated from the Fourier transform of the model coefficients. DTF values are obtained from the transfer matrix $\boldsymbol{H}(f)$, which is obtained by taking the inverse of the Fourier transform of the model coefficients $\boldsymbol{A}(f)$:

$$DTF_{ij} = \frac{|H_{ij}(f)|}{\sqrt{\sum_{m=1}^{M}|H_{im}(f)|^2}}, \quad (3)$$

where

$$H_{ij}(f) = \bar{A_{ij}}(f)^{-1}, \quad (4)$$

and

$$\boldsymbol{S}(f) = \mathbf{H}(f)\,\mathbf{V}\,\mathbf{H}^{*}(\mathrm{f}), \quad (5)$$

where **V** is the residual covariance matrix of noise process $w(n)$, $\boldsymbol{S}(f)$ is the spectral matrix of the signal, and $\mathbf{H}^{*}(f)$ is a Hermitian transpose of matrix $\mathbf{H}(f)$.

To accurately compute an MVAR model, we must determine the optimal model order. That is, we want to know how many time-lag terms to include in the MVAR model. Too few terms will result in a poor characterization of the original time series, and the associated power spectrum profile will be smooth and featureless. Too many terms results in over-fitting and can lead to spurious peaks in the power spectrum. The model order used in our analyses was determined by computing information-theoretic criteria and by comparing the parametric-computed power spectrum with the nonparametric-computed spectrum.

Several information-theoretic criteria were computed since they are based on different assumptions about the signal and use different methods to penalize the model for additional parameters (see Appendix B), including the Akaike Information Criterion (AIC), Hannan-Quin Criterion (HQIC), Bayesian Information Criterion (BIC), and Forward Prediction Error (FPE) (Akaike 1974; Akaike 1981; Stoica and Selen 2004; Blinowska-Cieślak and Zygierewicz 2012). Additionally, the versions of the AIC, BIC, and HQIC corrected for small sample sizes were computed: AICc, BICc, and HGIc. These 7 information-theoretic criteria were computed separately for each of the 6 network topologies examined in this study, and the results are shown in Fig. 2. The model order is determined by searching for a local minimum in the plots across the criteria. Due to different assumptions about the signal, some of them may not show the minimum, so the model order is selected from those plots that do have a minimum. Here, the minimum of the BIC, FPE, and adjusted BICc is approximately the same for all network topologies, so we chose a model order of $p = 10$. Each time lag is one sample of the time series data, so the MVAR model for each simulation examined whether or not the current signal can be predicted from the previous 10 samples from all other nodes. The appropriateness of $p = 10$ for these data was also examined by comparing the power spectrum computed using the auto-regressive model with one using Welch's method, and we obtained good agreement between the parametric $\boldsymbol{S}(f)$and nonparametric (Matlab's pwelch function) spectrum (Brovelli et al. 2004).

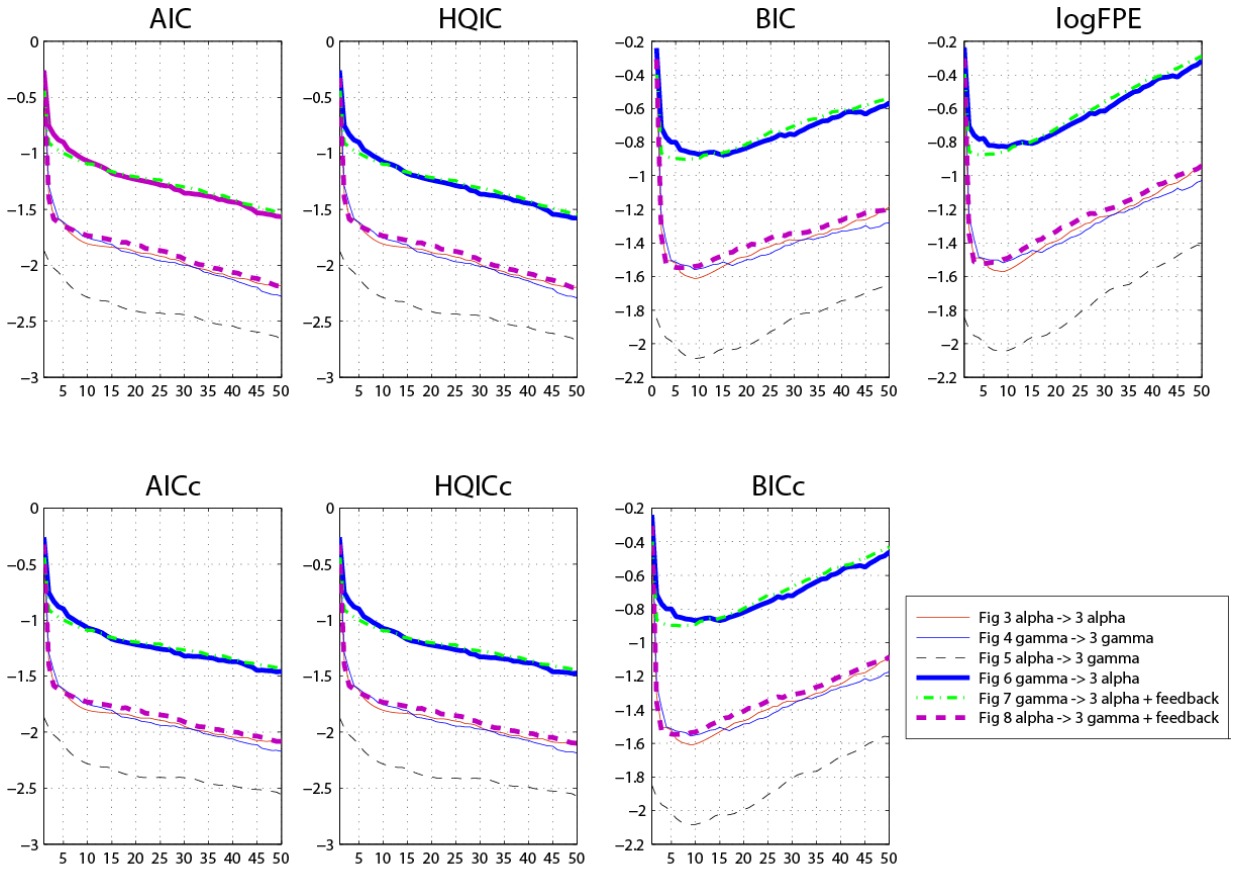

Fig. 2 Values of 7 information-theoretic criteria plotted against the model order used. The legend is labeled according to the figures in which the power spectra and associated DTF results for the simulated networks are presented.

In addition to computing the connectivity measure across all frequencies, we also integrated DTF only in the frequency ranges where the power spectrum shows peaks in our 2 bands of interest, alpha (10–12 Hz) and gamma (35–45 Hz). Theses ranges were determined by the full width at half-maximum value for the peak in power spectrum in the node where the peak in an alpha or gamma range was the highest.

2.3 Computing Statistical Significance

We determined statistical significance of the computed measures by shuffling the phase of the signals using Theiler's method (Prichard and Theiler 1994) to generate surrogate data. The advantage of the Theiler method is that it can be easily applied to experimentally obtained time series, our targeted use of this method in future research. The method takes the Fourier transform X(f) of the time series x(t) and multiplies each point by a random phase. We symmetrize X(f) and take the inverse Fourier transform, which results in signals that have the same power spectrum as the original signal but with no correlation in the phases (Blinowska-Cieślak and Zygierewicz 2012). This process was repeated 500 times on the signal obtained from the

connected network simulation, and we generated a histogram of the results. From this, we obtained the distribution of the DTF values for each frequency. We computed the 95th percentile for the distribution at each frequency point resulting in a significance level of $p < 0.05$.

3. Results

We computed connectivity values for each of our 6 simulated networks using DTF. In each figure, section A shows the network topology, section B shows the power spectrum $S_{ii}(f)$ between 0 and 100 Hz as computed from the MVAR model, and section C shows the computed DTF. The rows in section C correspond to the sending nodes whereas the columns correspond to the receiving nodes. In each DTF plot, the black curves correspond to the significance level computed using Theiler's method as described in Section 2.3 of this report, and the red curves above the black lines correspond to frequency values with DTF values that were statistically significant based on Theiler's method.

3.1 Simple Networks

All of these networks consisted of a central driving node that projects to 3 other receiving nodes. The parameters of the nodes were tuned so that the nodes would intrinsically oscillate either in the alpha band centered around 13 Hz or in the gamma range centered around 40 Hz. We examined the following 4 cases:

- An alpha frequency node drives 3 alpha frequency nodes.
- A gamma frequency node drives 3 gamma frequency nodes.
- An alpha frequency node drives 3 gamma frequency nodes.
- A gamma frequency node drives 3 alpha frequency nodes.

In the first simulation, an alpha frequency node drives 3 alpha frequency nodes, as shown in Fig. 3A, where node 1 acts as the driver of the other 3 nodes with simulated synaptic connections projecting to nodes 2–4. The power spectrum in Fig. 3B shows that node 1 has the most power but all nodes peak near 13 Hz. Figure 3C is the computed DTF between 0 and 100 Hz. In the top row of Fig. 3C are the DTF components corresponding to connections 1 → 2, 1 → 3, and 1 → 4. Given the underlying topology of the network, one would expect that only connections 1 → 2, 3, 4 would result in significant values of the DTF. However, we see that in 8 of the 9 other panels in this plot, the red DTF values are above the significance threshold shown in black. In particular, we see that the DTF is significant in components 4 → 1 and 4 → 3 across all frequencies except for a narrow band corresponding to the peak of the power spectrum (peaked near 14 Hz).

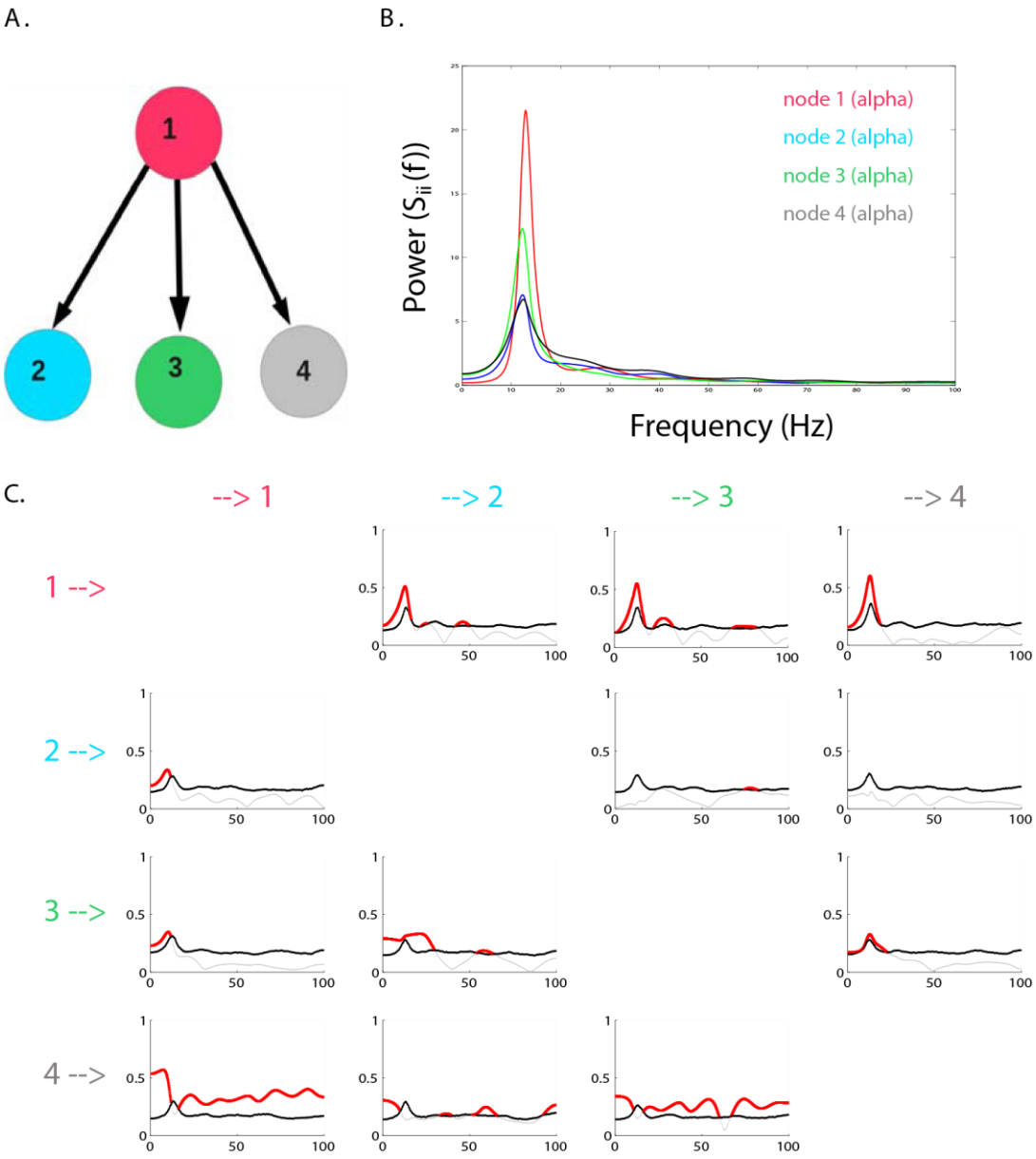

Fig. 3 Alpha node 1 driving 3 alpha nodes. A: connectivity structure of a simulated network. B: power spectrum (0–100 Hz) computed from the MVAR model. C: computed DTF values plotted against frequency (0–100 Hz), where the rows correspond to the sending nodes and the columns correspond to the receiving nodes. In each DTF plot, the red curves above the black lines correspond to frequency values with DTF values statistically significant.

The second simulation shown in Fig. 4 is identical to Fig. 3 except all nodes are now generating a signal in the gamma range. Similar to the first simulation, node 1 has much more power than the other 3 nodes, indicating a larger degree of synchrony. Examining the top row of Fig. 4C, we see that the components of the DTF corresponding to connections 1 → 2, 3, 4 are substantially above the level of significance for a wide range of frequencies, much more so than the same

components seen in Fig. 3C. This being said, there are still spurious results that indicate connections 3 → 1 and 2 → 3. If we examine the component of the DTF corresponding to the connection 1 → 3, we see that the measure is above significance over a broad range of frequencies. In fact, it is significant over a range of frequencies in which there is no power in the corresponding spectrum. It is impossible for there to be an influence from one region to another within this frequency band, and thus these results show that DTF detects spurious connections.

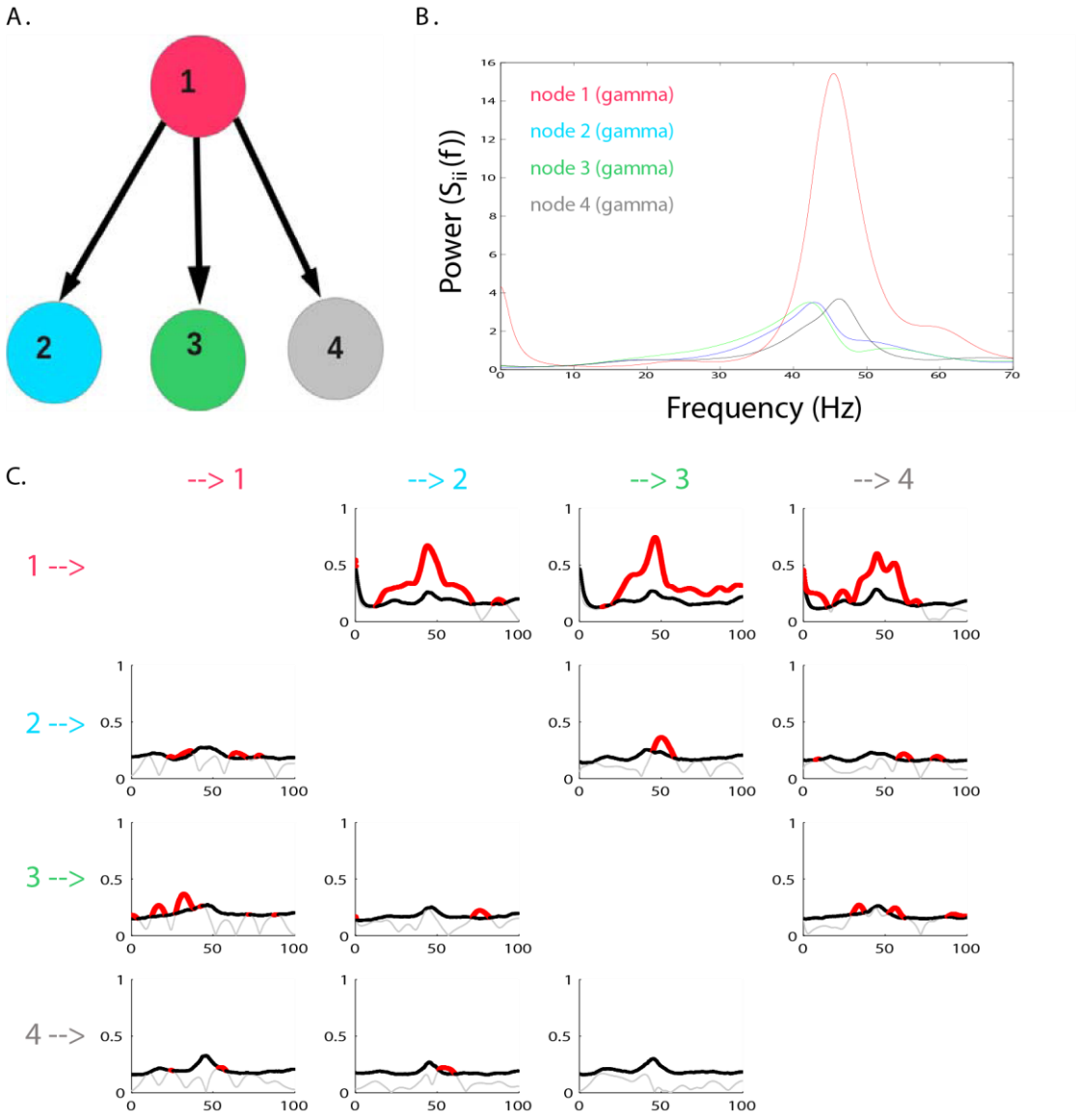

Fig. 4 Gamma node 1 driving 3 gamma nodes. A: connectivity structure of a simulated network. B: power spectrum (0–100 Hz) computed from the MVAR model. C: computed DTF values plotted against frequency (0–100 Hz), where the rows correspond to the sending nodes and the columns correspond to the receiving nodes. In each DTF plot, the red curves above the black lines correspond to frequency values with DTF values statistically significant.

Next we examined a situation where the driving node had little effect on the receiving nodes. Figure 5 is a simple network in which the driving node oscillates in the alpha frequency band and the receiving nodes oscillate in the gamma frequency band. Importantly, in the power spectrum plot shown in Fig. 5B, there is little overlap between the spectra of the sending and receiving nodes. Examining the 1 → 2, 3, 4 components of the DTF in Fig. 5C, the DTF values are not above significance in the frequency band of the driving node. The DTF is slightly above significance in the 1 → 2 and 1 → 3 components near 50 Hz.

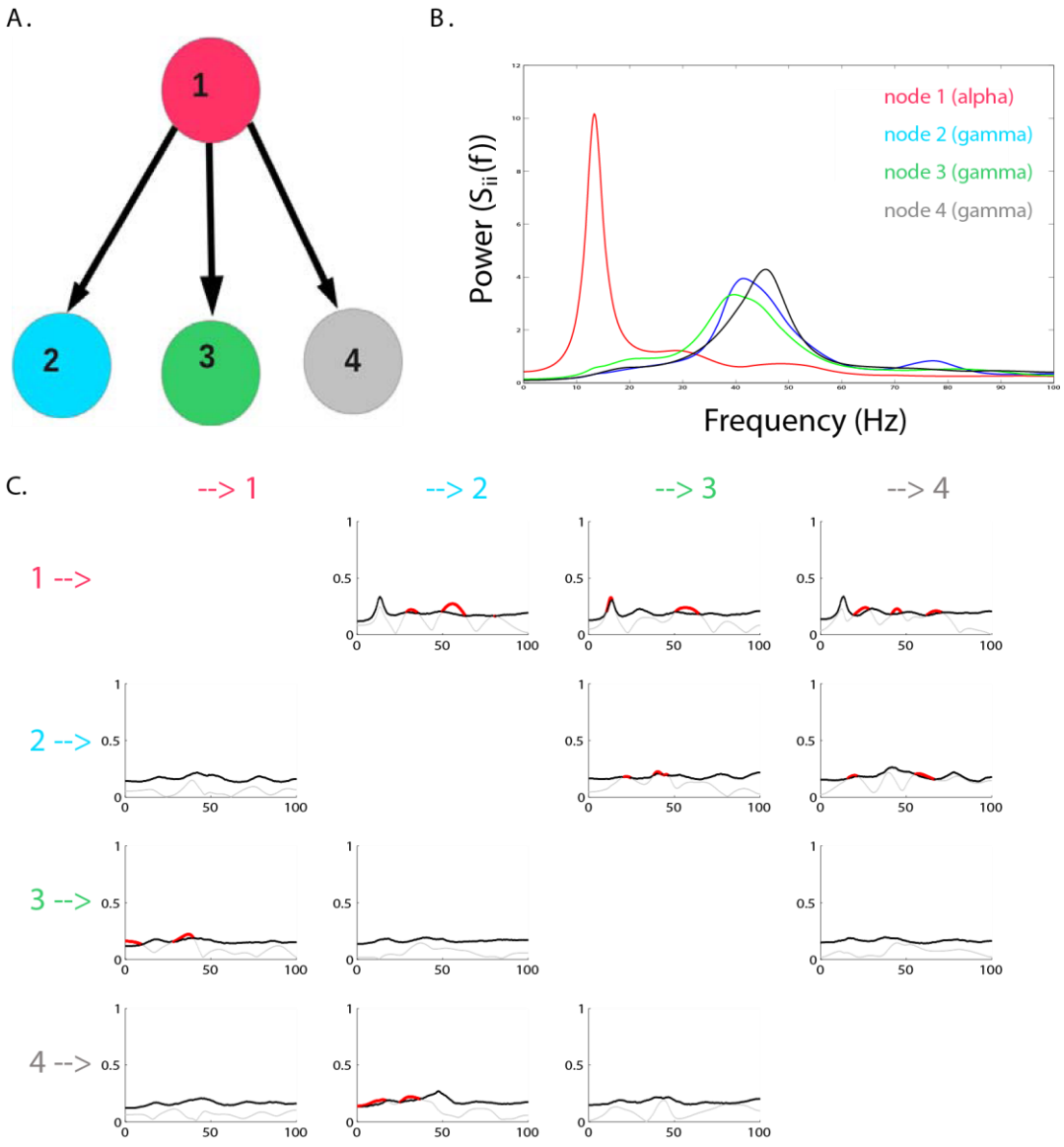

Fig. 5 Alpha node 1 driving 3 gamma nodes. A: connectivity structure of a simulated network. B: The power spectrum (0–100 Hz) computed from the MVAR model. C: computed DTF values plotted against frequency (0–100 Hz), where the rows correspond to the sending nodes and the columns correspond to the receiving nodes. In each DTF plot, the red curves above the black lines correspond to frequency values with DTF values statistically significant.

Finally, we examine a case in which the driving node oscillates in the gamma frequency range and the receiving nodes are tuned to oscillate in the alpha band range. The power spectrum is shown in Fig. 6B, and in this case we see that node 1 induces a large frequency component near 40 Hz in the receiving nodes. This increase in power is likely due to the entrainment of many neurons in the receiving node to the driving node's frequency. Examining the components of the DTF associated with these connections, we see that they are peaked near the 50-Hz region near the frequency of the driving oscillating node. Analogous to the case shown in Fig. 4 with nodes oscillating in the gamma frequency range, they are also all substantially above the significance level. There are 2 prominent, spurious components of the DTF indicating connections from nodes 4 → 2 and 4 → 3. In addition, we see that there are several components of the DTF that are significant at high frequencies even though there is no substantial power in the spectral plots.

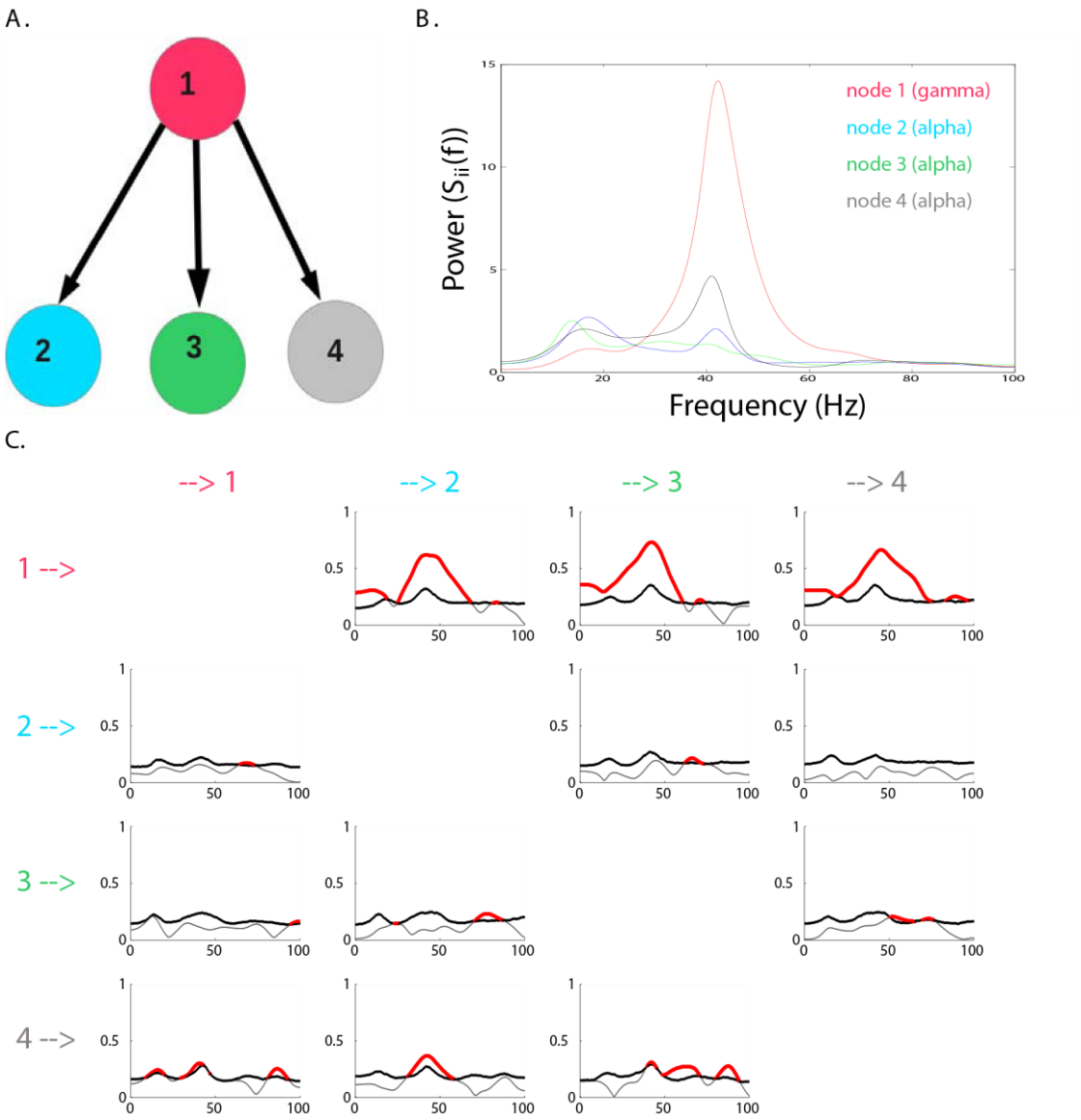

Fig. 6 Gamma node 1 driving 3 alpha nodes. A: connectivity structure of a simulated network. B: power spectrum (0–100 Hz) computed from the MVAR model. C: computed DTF values plotted against frequency (0–100 Hz), where the rows correspond to the sending nodes and the columns correspond to the receiving nodes. In each DTF plot, the red curves above the black lines correspond to frequency values with DTF values statistically significant.

3.2 Networks with Feedback Loops

These 2 networks consisted of a central driving node that projects to 3 other receiving nodes with feedback connections and a ring structure. Just like the simple networks, the parameters of the nodes were tuned so that the nodes would intrinsically oscillate either in the high alpha band from 10 to 15 Hz or in the gamma range around 40 Hz. We examined the following 2 cases with a mismatch in frequency between the driving and receiving nodes:

- A gamma frequency node drives 3 alpha frequency nodes with feedback and a ring connection.
- An alpha frequency node drives 3 gamma frequency nodes with feedback and a ring connection.

In the first simulation, a gamma frequency node 1 drives 3 alpha frequency nodes, as shown in Fig. 7, with feedback connections from 2 of the nodes (3 and 4) and an additional direct connection between nodes 2 and 4. The power spectrum in Fig. 7B shows that node 1 introduces substantial gamma frequency components in the power spectrum of its 3 receiving nodes. Thus the components of the DTF shown in Fig. 7C that correspond to connections from node 1 and projecting to nodes 2–4 are very prominent and substantially above the level of significance in the frequencies where power exists in the connected nodes. However, just as in Fig. 6, there are spurious connections detected as indicated by the significant DTF values at high frequencies (even 100 Hz) even though there is no substantial power in the power spectrum of any of the nodes at these frequencies.

The DTF values in Fig. 7C do not robustly capture the feedback connections from 3 and 4 to node 1. No significance is found in the connection 3 → 1, and the connection 4 → 1 is barely detected by the connectivity measure and only at the edge of the higher frequencies showing power in the spectral plot. The final connection 2 → 4 shows significant DTF values at both frequency ranges where power is seen in the spectral plot. Finally, there is a spurious connection detected projecting from node 2 to node 1. In this case, the DTF has peaks in both the alpha and the gamma range. These peaks correspond to the peaks of the power spectrum of the sending and receiving nodes. Even though there is a true connection from node 4 to node 1, the corresponding component of the DTF shows that node 4 has little influence on node 1. It is possible that this is an example of the activity of node 2 propagating around the ring to node 1. However, this does not seem likely since the spurious peaks are more significant than the 4 → 1 component.

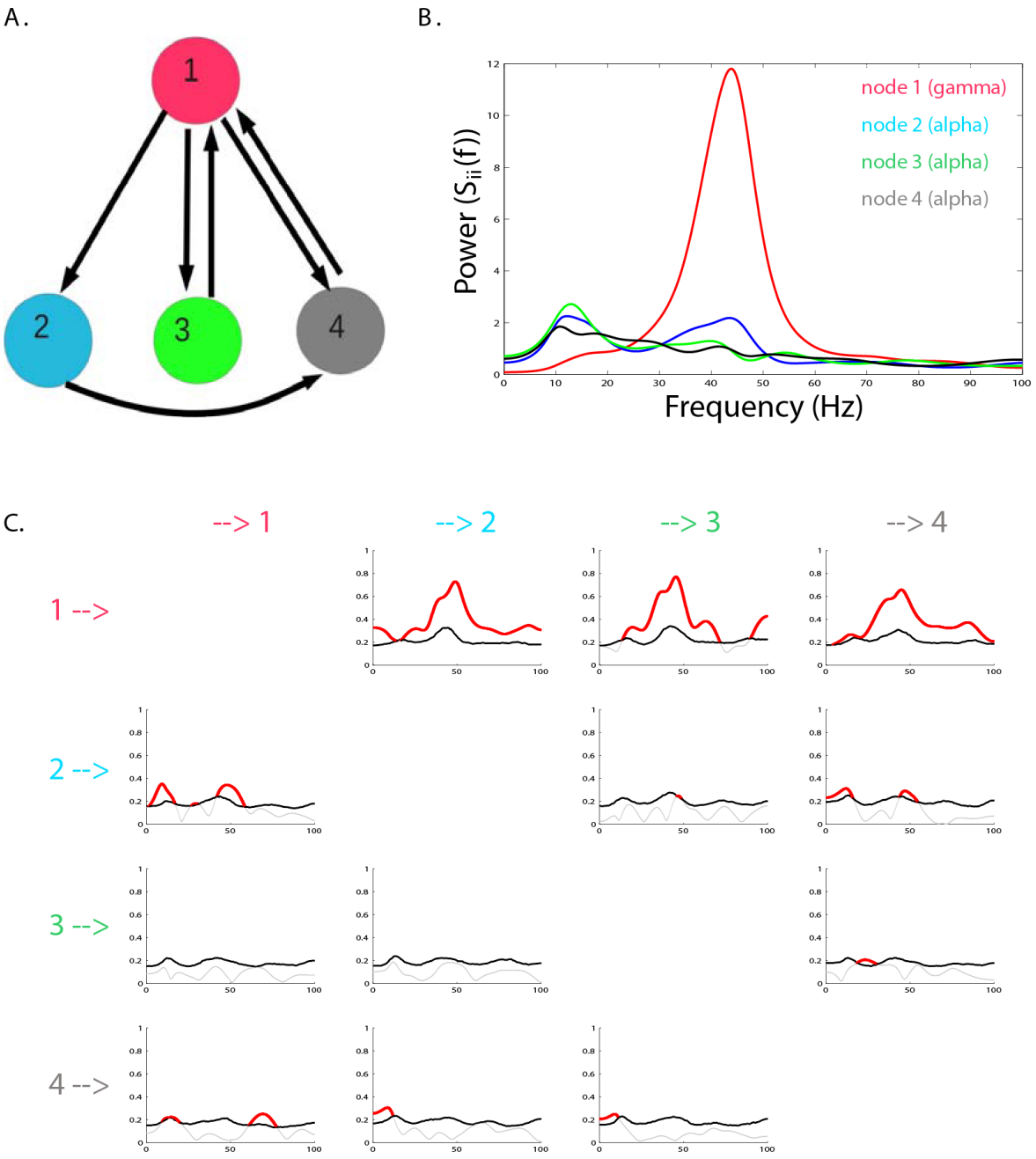

Fig. 7 Gamma node 1 driving 3 alpha nodes with feedback loop. A: connectivity structure of a simulated network. B: power spectrum (0–100 Hz) computed from the MVAR model. C: computed DTF values plotted against frequency (0–100 Hz), where the rows correspond to the sending nodes and the columns correspond to the receiving nodes. In each DTF plot, the red curves above the black lines correspond to frequency values with DTF values statistically significant.

The second simulated network in Fig. 8 has the same connectivity pattern as Fig. 7 but the oscillating frequencies of the nodes are switched: In this case, node 1 oscillates in the alpha band and nodes 2–4 oscillate in the gamma band. Here we see similar results as those obtained in the simple networks. Namely, when node 1 oscillates in the alpha band, it does not entrain a substantial portion of neurons of the higher oscillating frequency nodes. Thus there is substantially less overlap in the power spectra of the sending and receiving nodes. The resulting DTF components are not significant (1 → 3 and 4) or only slightly above the significance level at the higher frequencies of oscillation with substantial power in node 2 (1 → 2). However, the feedback connections (1 ← 3 and 4) and ring connection (2 → 4) from the nodes oscillating at the gamma frequency are captured relatively well, although frequencies outside the peaks of power in the spectral plot are shown as significant. Finally, we do have some spurious connections detected between (4 ←2) and the one seen in the first simulation in Fig. 7 between node 2 to node 1. This latter component of the DTF is actually more significant than what was observed in Fig. 7.

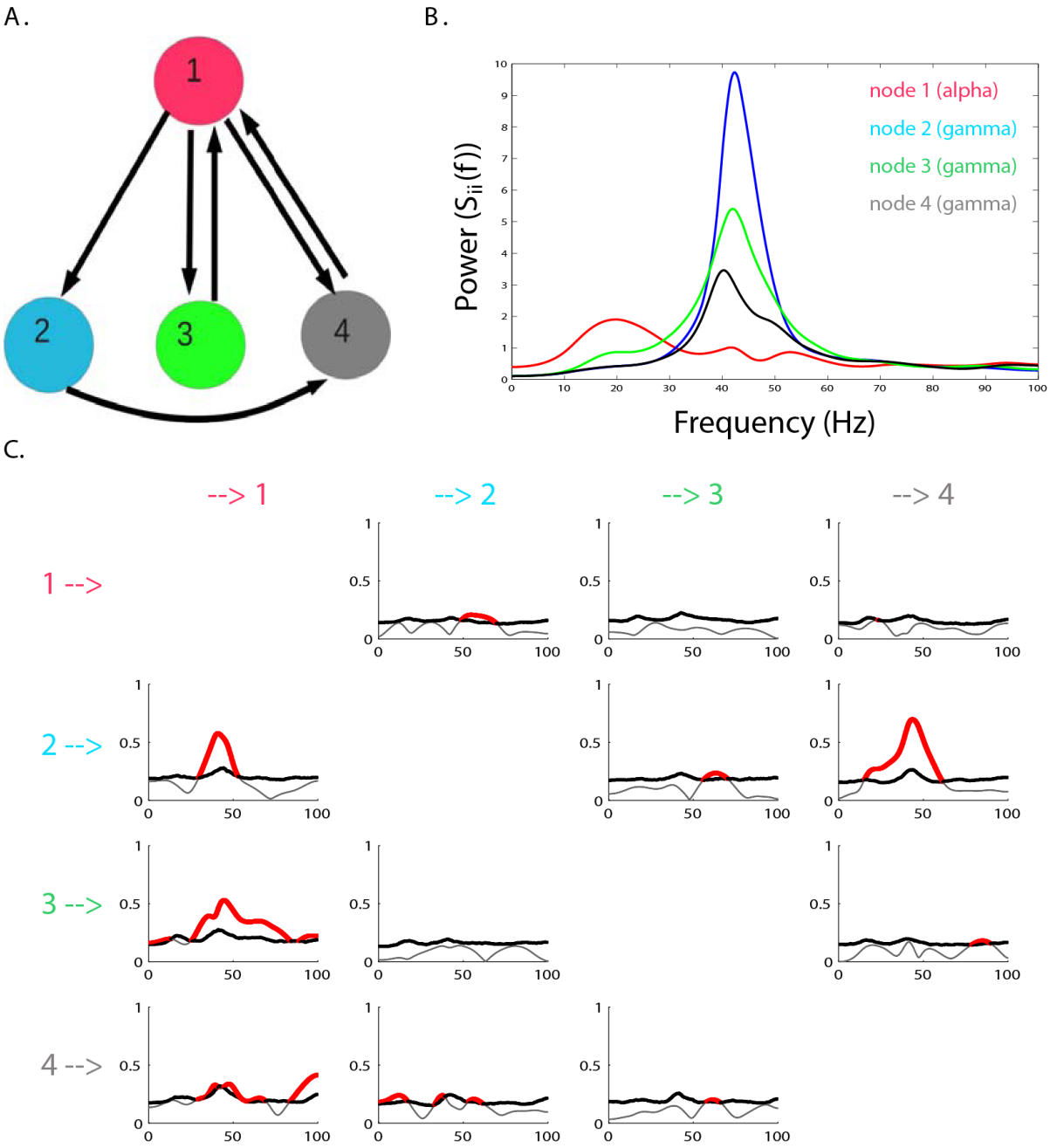

Fig. 8 Alpha node 1 driving 3 gamma nodes with feedback loop. A: connectivity structure of a simulated network. B: power spectrum (0–100 Hz) computed from the MVAR model. C: computed DTF values plotted against frequency (0–100 Hz), where the rows correspond to the sending nodes and the columns correspond to the receiving nodes. In each DTF plot, the red curves above the black lines correspond to frequency values with DTF values statistically significant.

3.3 Results Constrained by Spectral Power

Across all 6 simulated networks, spurious connections are detected; however, a majority of these spurious connections are detected at frequencies outside of the broadly tuned alpha and gamma oscillations of the network nodes. We propose that these false positives may be mitigated by examining the connectivity values only in frequencies that have clear power peaks in the spectrum indicating presence of rhythmic activity. For these test networks, the maximum of the power spectrum corresponds to the frequency around which most of the cells in the population are synchronized. Thus, we assume that the largest synchronized cluster of cells within a node will have the most prominent effect on the receiving nodes and minimal influence from the smaller clusters oscillating at different frequencies. Here, we constrain the analysis for each of the 6 simulations to the frequency range for alpha and gamma where the power spectrum shows peaks. The range of frequencies for this analysis was chosen as full width at half-maximum of the powers density in the node with the highest values in each frequency band, and we examine how this constraint influences the reliability of the DTF measure.

Figure 9 shows the DTF results of our 6 simulations for the peak in the alpha range (10–12 Hz) in light blue and the gamma range (35–45 Hz) in dark blue. Each panel represents the results for networks represented in previous figures (i.e., panel A is data from Fig. 3, panel B is Fig. 4, etc.).

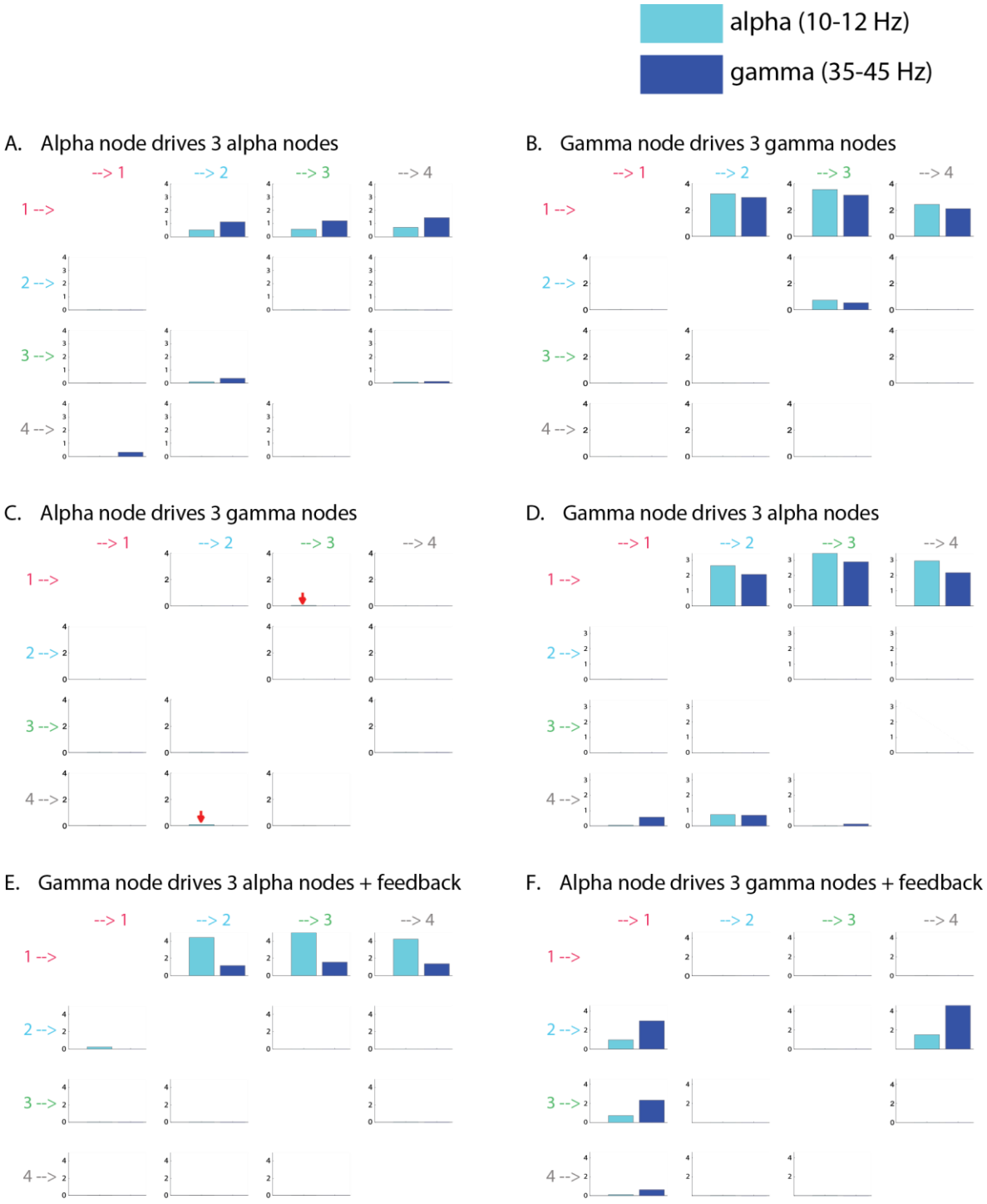

Fig. 9 The computed DTF values plotted against frequency, where the rows correspond to the sending nodes and the columns correspond to the receiving nodes. In all of these panels, the frequency bands used for integration of significant DTF values were chosen as 10–12 Hz for alpha band (light blue) and 35–45 Hz for gamma band (dark blue). In all panels, node 1 is the driving node. The integrals in each panel are labeled corresponding to their associated figure: A = Fig. 3, B = Fig. 4, C = Fig. 5, D = Fig. 6, E = Fig. 7, and F = Fig. 8.

The simple networks are shown in panels A–D where one driving node projects to 3 other receiving nodes. The first 2 networks in panels A and B have driving and receiving nodes that oscillate at the same intrinsic frequency. As such, they have strongly overlapping spectra, and their connectivity pattern is captured relatively well by the DTF measure. While there are some spurious connections indicated as significant with Theiler method, the real connection from node 1 to all others is clearly dominant in both integrated frequency ranges. However, the same network connectivity is shown in panels C and D but with a difference in intrinsic frequency of oscillations between driving and receiving nodes, and this configuration shows a different connectivity pattern. In panel C, the driving node oscillates at a frequency in the alpha range and the receiving nodes oscillate in the gamma range. This configuration is not detected well by DTF, with mildly significant DTF values for only one of the 3 actual connection (1 → 3) and a spurious connection (4 → 2). In panel D, the frequency bands flip from panel C with the driving node oscillating in the gamma range and receiving nodes in the alpha range. This configuration is detected substantially better than in C, matching the levels of significance seen with a pure gamma network in panel B. The real connection from node 1 to all others is clearly dominant in both the integrated frequency ranges and the much smaller significance values for the spurious connections from (4 → 1 and 2).

The more complex networks with feedback connections and a ring structure are shown in panels E–F. These last 2 panels show that significant DTF values do not correctly represent the underlying connectivity. In panel E, the connectivity pattern showing node 1 as driving all others is reproduced with higher DTF values in alpha band despite node 1 dominant oscillations in gamma band. The feedback connections (3 and 4 → 1) and connection 2 → 4 are not detected, but the spurious connection (2 → 1) is captured with a barely significant DTF value in the alpha range. In panel F, when node 1 is oscillating in alpha range, the connectivity is misrepresented to the largest degree. Node 1 is correctly shown to receive input not only from nodes 3 and 4, but also incorrectly shown as receiving input from node 2. The connection 2 → 4 is correctly detected; however, the connections 1 → 2, 3, 4 are not detected at all.

4. Discussion

In this study, we simulate 6 networks using conductance-based model neurons that oscillate in frequency bands commonly investigated in experimental EEG studies, alpha and gamma (Nunez and Srinivasan 2006). Four of these simulated networks have a simple feed-forward structure with one node driving the other 3, and 2 have a more complex connectivity structure with additional feedback connections and a ring structure. Across all 6 simulated configurations, we manipulate whether the driving nodes oscillate at alpha or gamma. The time series from each simulated network is separately fit to an MVAR model, and an effective connectivity measure,

DTF, is computed from the model coefficients. Our analysis examined how well this effective connectivity measure captured the underlying functional connectivity of the network to assess its utility for recovering network connections in experimental EEG data in future research.

Our results demonstrate that these functional connectivity measures can provide useful information about causal influences among network nodes, but they should be applied conservatively and interpreted carefully since they detect spurious connections even in simplified network configurations. We propose 2 guiding principles for application and interpretation of these measures on experimental EEG data: 1) analyze only those frequency bands with substantial overlap in the power spectra of the experimental recordings from investigated nodes and 2) apply a conservative statistical threshold. The measures performed best on the simple feed-forward networks, so they are likely most applicable for recovering less complicated network interactions and may perform better when knowledge about anatomical connections can be used to constrain their application or interpretation.

Across these 6 simulations, the measures correctly identify connections when the driving node induces substantial activity in the same frequency as the receiving node, resulting in significant overlap of power spectra of both nodes. This effect was evidenced in both simple networks with all nodes oscillating in the same frequency band (alpha in Fig. 3 and gamma in Fig. 4) and when the driving node entrained the receiving nodes, which was more common for nodes oscillating in the gamma frequency (Figs. 6 and 8). Likewise, in Fig. 5, there was not much overlap in the alpha power spectrum and DTF was minimally significant and did not reliably capture the connectivity among the nodes. This overall difference between alpha and gamma oscillations may heavily depend on the dynamics of the networks in question. In our model, afferent connections from a network oscillating at a high frequency to a network oscillating at a lower frequency are detected at a much weaker coupling strength than in the opposite scenario. Thus, our model networks have a preference for higher frequency inputs, and this highlights a critical element of our results: the importance of power overlap in the spectrum.

Our results show that entrainment between the nodes is not limited to their dominant oscillating frequency. The measure also detected connectivity in other frequency ranges since the driving node may synchronize over the total activity in the receiving node so the effective connectivity is visible across the whole frequency range. Consequently, we propose that the analysis should be constrained only to those frequencies with overlapping power in the spectrum. This enhanced the level of significance for the connectivity values, as demonstrated in Fig. 9.

Of course limiting the analysis to overlapping power in the spectrum may miss some real connections. In an experimental data set there may be synchronous activity in a frequency band not corresponding to the maximum of the power spectrum (Brovelli et al. 2004). In this case, the ability of one population of cells to entrain another at a certain frequency is dependent both on anatomical connectivity as well as the biological properties of the cells involved in the

oscillation. In such cases, one would have to employ a variety of information to attempt to infer the effective connections, including any details about the true anatomical connectivity between cell populations and brain regions.

Although implementing a constraint based on the power spectrum improves the performance of the connectivity measures, using a statistical method with significance level 0.05 still shows some spurious connections. In more complicated networks, when subnetworks at each node have different levels of synchrony or oscillate at different frequencies, the measures may function less reliably. This was evident in Figs. 7 and 8, which indicated an influence from node 2 to node 1 where no connection exists. To maximize the correct number of detected connections, one must not only examine the measures in a narrow band around the peak of the power spectrum, but also set a relatively conservative significance level. Future work should examine if alternative statistical approaches or surrogate data approaches can improve identification of spurious connections.

When interpreting connectivity analyses of experimental data, these connectivity measures are likely best used to confirm a hypothesis about effective connectivity based on some other anatomical and physiological data. These measures are not well suited to be used in isolation to try and determine unknown anatomical connections, but they can likely reveal dynamic casual interactions between brain regions when there is already some knowledge to formulate hypotheses about the underlying network connectivity. Previous research has shown that bivariate Granger Causality fails to correctly detect functional connections in a simple Pyloric central pattern generator (Kispersky et al. 2011). They computed the Granger Causality measure on a time series obtained from the stomato-gastric ganglion of the crab, which consists of 3 oscillating subpopulations of neurons. They found that the computed Granger Causality inferred casual influences where no anatomical connections exist (Kispersky et al. 2011). Thus, our results are complementary and suggest that methods based on autoregressive modeling can produce spurious results when feedback connections are introduced into a network or when the network is more complicated than a simple network with a single source projecting to other nodes.

Furthermore, these linear methods are prone to error simply from the fact that we are attempting to fit a time series generated from a nonlinear process to a linear model. Thus, this may be another reason that we detect spurious connections. In particular, DTF and similar methods reliant on computations in the frequency domain are unable to detect cross-frequency interactions, but in nonlinear systems like the brain, there might be interactions between systems not inducing the same frequency activity in the receiving node. Future research should examine nonlinear alternatives for recovering functional connectivity patterns.

5. Conclusion

Our simulations suggest the directed connectivity measures should be interpreted carefully and applied conservatively to experimental EEG datasets. We suggest 2 guiding principles for experimental analyses. First, DTF should only be analyzed in a frequency band centered at the frequency ranges with substantial overlap in the power spectra of the signals from different brain regions. Second, a conservative estimate of the significance should be used to avoid detecting spurious connections.

Although these guiding principles will not completely eliminate spurious results, they may greatly reduce the number of false positives. These measures may be particularly helpful when testing hypotheses about connectivity among known anatomical structures, but they are unlikely to be informative when trying to infer underlying, unknown connectivity. Additional measures such as phase-synchronization measures or measures based on autoregressive models with time-dependent coefficients may be further used as a check on the validity of the results obtained with measures similar to DTF. The inclusion of such measures may provide yet another way to bolster our criterion for validating whether or not 2 brain regions are interacting.

6. References

Akaike H. A new look at the statistical model identification. IEEE Transactions on Automatic Control. 1974;19(6):716–723. doi:10.1109/TAC.1974.1100705.

Akaike H. Likelihood of a model and information criteria. Journal of Econometrics. 1981;16(1):3–14.

Alivisatos AP, Chun M, Church GM, Greenspan RJ, Roukes ML, Yuste R. The brain activity map project and the challenge of functional connectomics. Neuron. 2012;74(6):970–974. doi:10.1016/j.neuron.2012.06.006.

Anderson WS, Azhar F, Kudela P, Bergey GK, Franaszczuk PJ. Epileptic seizures from abnormal networks: why some seizures defy predictability. Epilepsy Research. 2012;99,202–213.

Baccalá LA, Sameshima K. Partial directed coherence: a new concept in neural structure determination. Biological Cybernetics. 2001;84(6):463–474.

Battaglia D, Witt A, Wolf F, Geisel T. Dynamic effective connectivity of inter-areal brain circuits. PLoS Comput Biol. 2012;8(3):e1002438. doi:10.1371/journal.pcbi.1002438.

Blinowska-Cieślak KJ, Zygierewicz J. Practical biomedical signal analysis using MATLAB. Boca Raton (FL): CRC Press, 2012.

Blinowska KJ, Kaminski M, Brzezicka A, Kaminski J. Application of directed transfer function and network formalism for the assessment of functional connectivity in working memory task. Philosophical Transactions of the Royal Society A: Mathematical, Physical and Engineering Sciences. 2013;371(1997):20110614. doi:10.1098/rsta.2011.0614.

Blinowska KJ. Review of the methods of determination of directed connectivity from multichannel data. Med Biol Eng Comput. 2011;49(5):521–529. doi:10.1007/s11517-011-0739-x.

Brovelli A, Ding M, Ledberg A, Chen Y, Nakamura R, Bressler SL. Beta oscillations in a large-scale sensorimotor cortical network: directional influences revealed by Granger causality. Proceedings of the National Academy of Sciences. 2004;101(26):9849–9854. doi:10.1073/pnas.0308538101.

Buschman TJ, Denovellis EL, Diogo C, Bullock D, Miller EK. Synchronous oscillatory neural ensembles for rules in the prefrontal cortex. Neuron. 2012;76(4):838–846. doi:10.1016/j.neuron.2012.09.029.

David O, Friston KJ. A neural mass model for MEG/EEG. NeuroImage. 2003;20(3):1743–1755. doi:10.1016/j.neuroimage.2003.07.015.

Engel AK, Fries P, Singer W. Dynamic predictions: oscillations and synchrony in top-down processing. Nature Reviews Neuroscience. 2001;2(10):704–716. doi:10.1038/35094565.

Friston KJ. Functional and effective connectivity: a review. Brain Connect. 2011;1(1):13–36. doi:10.1089/brain.2011.0008.

Geweke J. Measurement of linear dependence and feedback between multiple time series. Journal of the American Statistical Association. 1982;77(378):304–313. doi.10.1080 /01621459.1982.10477803.

Golub GH, Loan CFV. Matrix computations. Baltimore (MD): The Johns Hopkins University Press, 2012.

Granger C. Investigating causal relations by econometric models and cross-spectral methods. Econometrica. 1969;37(3):424–438. doi:10.2307/1912791.

Haufe S, Nikulin VV, Müller KRR, Nolte G. A critical assessment of connectivity measures for EEG data: a simulation study. Neuroimage. 2013;64,120–33. doi:10.1016/j.neuroimage .2012.09.036.

Ioannides AA, Dimitriadis SI, Saridis GA, Voultsidou M, Poghosyan V, Liu L, Laskaris NA. Source space analysis of event-related dynamic reorganization of brain networks. Computational and Mathematical Methods in Medicine. 2012;12:15 pages online. Article ID No.: 452503. doi:10.1155/2012/452503.

Jensen O, Bonnefond M, VanRullen R. An oscillatory mechanism for prioritizing salient unattended stimuli: trends in cognitive sciences. 2012;16(4):200–206. doi:10.1016 /j.tics.2012.03.002.

Kispersky T, Gutierrez GJ, Marder E. Functional connectivity in a rhythmic inhibitory circuit using Granger causality. Neural Systems and Circuits. 2011;1(1):9. doi:10.1186/2042-1001 -1-9.

Klimesch W, Sauseng P, Hanslmayr S, Gruber W, Freunberger R. Event-related phase reorganization may explain evoked neural dynamics. Neuroscience and Biobehavioral Reviews. 2007;31(7):1003–1016. doi:10.1016/j.neubiorev.2007.03.005.

Korzeniewska A, Mańczak M, Kamiński M, Blinowska KJ, Kasicki S. Determination of information flow direction among brain structures by a modified directed transfer function (dDTF) method. Journal of Neuroscience Methods. 2003;125(1):195–207.

Kudela P, Franaszczuk PJ, Bergey GK. A simple computer model of excitable synaptically connected neurons. Biological Cybernetics. 1997;77(1):71–77.

Nunez PL, Srinivasan R. Electric fields of the brain: the neurophysics of EEG. Oxford (UK): Oxford University Press, 2006.

Philiastides MG, Sajda P. Causal influences in the human brain during face discrimination: a short-window directed transfer function approach. IEEE Transactions on Biomedical Engineering. 2006;53(12):2602–2605. doi:10.1109/TBME.2006.885122.

Prichard D, Theiler J. Generating surrogate data for time series with several simultaneously measured variables. Physical Review Letters. 1994;73(7):951–954. doi:10.1103 /PhysRevLett.73.951.

Sakkalis V. Review of advanced techniques for the estimation of brain connectivity measured with EEG/MEG. Computers in Biology and Medicine. 2011;41(12):1110–1117. doi:10.1016/j.compbiomed.2011.06.020.

Schiff S, So P, Chang T, Burke R, Sauer T. Detecting dynamical interdependence and generalized synchrony through mutual prediction in a neural ensemble. Physical Review E, Statistical Physics, Plasmas, Fluids, and Related Interdisciplinary Topics. 1996;54(6):6708–6724.

Seghouane AK, Amari SI. Identification of directed influence: Granger causality, Kullback-Leibler divergence, and complexity. Neural Computation. 2012;24(7):1722–1739. doi:10.1162/NECO_a_00291.

Sporns O, Chialvo DR, Kaiser M, Hilgetag CC. Organization, development and function of complex brain networks. Trends Cogn Sci. 2004;8(9):418–425. doi:10.1016/j.tics2004 .07.008.

Stoica P, Selen Y. Model-order selection: a review of information criterion rules. IEEE Signal Processing Magazine. 2004;21(4):36–47. doi:10.1109/MSP.2004.1311138.

Suffczynski P, Crone NE, Franaszczuk P. Afferent inputs to cortical fast-spiking interneurons organize pyramidal cell network oscillations at high-gamma frequencies (60–200 Hz). Journal of Neurophysiology. 2014;112(11):3001–3011. doi:10.1152/jn.00844.2013

Sun Y, Zhang H, Feng T, Qiu Y, Zhu Y, Tong S. Early cortical connective network relating to audiovisual stimulation by partial directed coherence analysis. IEEE Transactions on Biomedical Engineering. 2009;56(11):2721–2724. doi:10.1109/TBME.2009.2025966.

Supp GG, Schlögl A, Fiebach CJ, Gunter TC, Vigliocco G, Pfurtscheller G, Petsche H. Semantic memory retrieval: cortical couplings in object recognition in the N400 window: cortical couplings in object recognition. European Journal of Neuroscience. 2005;21(4):1139–1143. doi:10.1111/j.1460-9568.2005.03906.x.

Varela F, Lachaux JP, Rodriguez E, Martinerie J. The brainweb: phase synchronization and large-scale integration. Nature Reviews Neuroscience. 2001;2(4):229–239. doi:10.1038 /35067550.

Wendling F, Ansari-Asl K, Bartolomei F, Senhadji L. From EEG signals to brain connectivity: a model-based evaluation of interdependence measures. Journal of Neuroscience Methods. 2009;183(1):9–18. doi:10.1016/j.jneumeth.2009.04.021.

Appendix A. Cortical Network Model

The following are the values of the parameters used in the neuron model based on the model developed by Kudela et al.[1,2] The individual channel currents are described by the following equations:

$$\begin{aligned} I_{Na} &= g_{Na} m_{\infty}^{3} V(1-W)(V-V_{Na}), \\ I_{Ca} &= g_{Ca} X^{2} \frac{K_c}{K_c+C}(V-V_{Ca}), \\ I_{K} &= g_{K} W^{4}(V-V_{K}), \\ I_{A} &= g_{A} A_{\infty}(V) B (V-V_{K}), \end{aligned} \tag{1}$$

and

$$I_L = g_L(V - V_L).$$

The recovery and activation variables for the previous equations are described by

$$\frac{dF}{dt} = \frac{F_{\infty}(V)-F}{\tau_F}, \tag{2}$$

where *F* represents *W*, *X*, *A*, *m*, and *B*. The steady state functions for these variables are given by an expression of the form

$$F_{\infty}(V) = \frac{1}{1+exp\left(-2a^{F}\left(V-V_{1/2}^{F}\right)\right)}. \tag{3}$$

In all equations, *V* is the neural membrane potential.

The synaptic current I_{syn} is modeled as

$$I_{syn}(t) = \sum_{j=1}^{N_{syn}} w_j g_j\left(t-\tau_j\right)\left(V_{rest} - E_{syn}^{j}\right), \tag{4}$$

where

$$g_j(t) = g_{syn} \sum_{k=1}^{N(t)} \left(exp((t_k - t)/\tau_d) - exp((t_k - t)/\tau_o)\right), \tag{5}$$

where *k* denotes summation over past action potentials on a given synapse and *j* denotes summation over all synaptic inputs of the neuron.

The values of conductances and reversal potentials used in the model neuron are as in Kudela et al.[2]

[1]Kudela P, Franaszczuk PJ, Bergey GK. A simple computer model of excitable synaptically connected neurons. Biological Cybernetics. 1997;77(1):71–77.

[2]Kudela P, Franaszczuk PJ, Bergey GK. Changing excitation and inhibition in simulated neural networks: effects on induced bursting behavior. Biological Cybernetics. 2003;88(4):276–285. doi:10.1007/s00422-002-0381-7.

In Table A-1 are listed the values that specify the number and types of connections between the excitatory and inhibitory neural subnetworks. Node connections are listed in Table A-2.

Table A-1 Parameter values for normal alpha activity in each subnetwork

Connection Type	**Domain Size**	**Connections Strength STD Delay STD**
Excitatory to excitatory	4 × 4	30 5 3 100 50
Excitatory to inhibitory	4 × 4	30 20 10 100 50
Inhibitory to excitatory	4 × 4	30–100 50 100 50
Inhibitory to inhibitory	4 × 4	5–100 75 100 50

Note: STD is a standard deviation of Gaussian distribution of the parameters.

Table A-2 Connections between nodes

Connection Type	**Domain Size**	**Connections Strength STD Delay STD**
Excitatory to excitatory	1 × 1	30 100 110 150 50
Excitatory to inhibitory	1 × 1	10 100 110 150 50
Inhibitory to excitatory	1 × 1	10–60 110 150 50
Inhibitory to inhibitory	1 × 1	20–60 110 150 50

INTENTIONALLY LEFT BLANK.

Appendix B. Multivariate Autoregressive Modeling (MVAR) Model

The formulas for MVAR model order selection criteria used in this study are the following:

$$AIC(p) = log\big(det(V)\big) + 2\frac{K(p)}{N}, \quad (1)$$

$$BIC(p) = log\big(det(V)\big) + \frac{log(N)K(p)}{N}, \quad (2)$$

$$HQIC(p) = log\big(det(V)\big) + \frac{log\big(log(N)\big)K(p)}{N},$$

and

$$log\big(FPE(p)\big) = log\left(det\big(V(p)\big)\right) + log\left(\frac{1+K(p)/N}{1-K(p)/N}\right), \quad (3)$$

$$AICc(p) = AIC(p) + 2\frac{K(p)(K(p)+1)}{N-K(p)-1}, \quad (4)$$

$$BICc(p) = BIC(p) + \frac{\log(N-K(p)-1)K(p)(K(p)+1)}{(\mathrm{N}-\mathrm{K(p)}-1)}, \quad (5)$$

$$HQICc(p) = HQICc(p) + \frac{\log(log(N-K(p)-1))K(p)(K(p)+1)}{(N-K(p)-1)}. \quad (6)$$

In these equations, $K(p) = pM^2+M(M+1)/2$ is a number of coefficients estimated for the model order p for M channels, and N is the number of sample points used in estimation. All of the model order selection criteria are derived under the assumption that the data in the time series x(n) is Gaussian distributed.[1]

Stoica P, Selen Y. Model-order selection: a review of information criterion rules. IEEE Signal Processing Magazine. 2004;21(4):36–47. doi:10.1109/MSP.2004.1311138.

1 (PDF) DEFENSE TECHNICAL INFORMATION CTR DTIC OCA

2 (PDF) DIRECTOR US ARMY RESEARCH LAB RDRL CIO LL IMAL HRA MAIL & RECORDS MGMT

1 (PDF) GOVT PRINTG OFC A MALHOTRA

1 (PDF) ARMY RSCH LABORATORY – HRED RDRL HRM D T DAVIS BLDG 5400 RM C242 REDSTONE ARSENAL AL 35898-7290

1 (PDF) ARMY RSCH LABORATORY – HRED RDRL HRS EA DR V J RICE BLDG 4011 RM 217 1750 GREELEY RD FORT SAM HOUSTON TX 78234-5002

1 (PDF) ARMY RSCH LABORATORY – HRED RDRL HRM DG J RUBINSTEIN BLDG 333 PICATINNY ARSENAL NJ 07806-5000

1 (PDF) ARMY RSCH LABORATORY – HRED ARMC FIELD ELEMENT RDRL HRM CH C BURNS THIRD AVE BLDG 1467B RM 336 FORT KNOX KY 40121

1 (PDF) ARMY RSCH LABORATORY – HRED AWC FIELD ELEMENT RDRL HRM DJ D DURBIN BLDG 4506 (DCD) RM 107 FORT RUCKER AL 36362-5000

1 (PDF) ARMY RSCH LABORATORY – HRED RDRL HRM CK J REINHART 10125 KINGMAN RD BLDG 317 FORT BELVOIR VA 22060-5828

1 (PDF) ARMY RSCH LABORATORY – HRED RDRL HRM AY M BARNES 2520 HEALY AVE STE 1172 BLDG 51005 FORT HUACHUCA AZ 85613-7069

1 (PDF) ARMY RSCH LABORATORY – HRED RDRL HRM AP D UNGVARSKY POPE HALL BLDG 470 BCBL 806 HARRISON DR FORT LEAVENWORTH KS 66027-2302

1 (PDF) ARMY RSCH LABORATORY – HRED RDRL HRM AT J CHEN 12423 RESEARCH PKWY ORLANDO FL 32826-3276

1 (PDF) ARMY RSCH LAB – HRED HUMAN SYSTEMS INTEGRATION ENGR TACOM FIELD ELEMENT RDRL HRM CU P MUNYA 6501 E 11 MILE RD MS 284 BLDG 200A WARREN MI 48397-5000

1 (PDF) ARMY RSCH LABORATORY – HRED FIRES CTR OF EXCELLENCE FIELD ELEMENT RDRL HRM AF C HERNANDEZ 3040 NW AUSTIN RD RM 221 FORT SILL OK 73503-9043

1 (PDF) ARMY RSCH LABORATORY – HRED RDRL HRM AV W CULBERTSON 91012 STATION AVE FORT HOOD TX 76544-5073

1 (PDF) ARMY RSCH LABORATORY – HRED RDRL HRM DE A MARES 1733 PLEASONTON RD BOX 3 FORT BLISS TX 79916-6816

8 (PDF) ARMY RSCH LABORATORY – HRED SIMULATION & TRAINING TECHNOLOGY CENTER RDRL HRT COL G LAASE RDRL HRT I MARTINEZ RDRL HRT T R SOTTILARE RDRL HRT B N FINKELSTEIN RDRL HRT G A RODRIGUEZ RDRL HRT I J HART RDRL HRT M C METEVIER RDRL HRT S B PETTIT 12423 RESEARCH PARKWAY ORLANDO FL 32826

1 (PDF) ARMY RSCH LABORATORY – HRED HQ USASOC RDRL HRM CN R SPENCER BLDG E2929 DESERT STORM DRIVE FORT BRAGG NC 28310

1 ARMY G1
(PDF) DAPE MR B KNAPP
300 ARMY PENTAGON RM 2C489
WASHINGTON DC 20310-0300

12 DIR USARL
(PDF) RDRL HR
L ALLENDER
P FRANASZCZUK
RDRL HRM
P SAVAGE-KNEPSHIELD
RDRL HRM AL
C PAULILLO
RDRL HRM B
J GRYNOVICKI
RDRL HRM C
L GARRETT
RDRL HRS
J LOCKETT
RDRL HRS B
M LAFIANDRA
RDRL HRS C
K MCDOWELL
J VETTEL
RDRL HRS D
A SCHARINE
RDRL HRS E
D HEADLEY